applied optics

Simulation of a simultaneous traceable spectroradiometric calibration of an imaging spectrometer

Simon A. Trim,[1,*] Jim Buffat,[2] and Andreas Hueni[1]

[1]Remote Sensing Laboratories (RSL), Department of Geography, University of Zurich, Winterthurerstrasse 190, 8057 Zurich, Switzerland
[2]Forschungszentrum Jülich Institutes IAS-8: Data Analytics and Machine Learning and IBG-2: Plant Sciences, Wilhelm-Johnen-Strasse, 52428 Jülich, Germany
*simon.trim@geo.uzh.ch

Received 6 November 2024; revised 18 December 2024; accepted 27 December 2024; posted 1 January 2025; published 22 January 2025

Spectroradiometric calibration aims to determine the instrumental spectral response function (ISRF) parameters and radiometric coefficients of an instrument's spectral bands across all spatial pixels. Typically, this is done by making separate spectral and radiometric calibration measurements. We present a method for the simultaneous traceable spectroradiometric calibration of an imaging spectrometer, using the Spectroscopically Tunable Absolute Radiometric, calibration and characterisation, Optical Ground Support Equipment (STAR-cc-OGSE) facility. We performed the forward simulation of calibration data acquisition by convolving input spectra with the sensor model's response and simulated a slit scattering function (SSF)-based calibration, allowing for both ISRF coefficients and the absolute spectral responsivities to be accurately retrieved from a single series of measurements. We show how the SSF method minimizes uncertainties compared to the traditional spectroradiometric calibration approach.

https://doi.org/10.1364/AO.547144

1. INTRODUCTION

Imaging spectrometers are used in multispectral and hyperspectral (hundreds or even thousands of narrow, adjacent spectral bands) imaging for a wide range of applications [1]. Earth observation (EO) has particularly benefited from technological developments in this field, generating vast data volumes [2]. Ideally, EO data can be traced back to a metrological reference through an unbroken chain of calibrations, each contributing to the stated measurement uncertainty [3,4].

For airborne and spaceborne instruments, calibration includes laboratory calibration prior to launch, in-flight or in-orbit calibration, and vicarious calibration [5]. The calibration process involves comparing the measurement values provided by a device under test with those of a calibrated standard of known uncertainty. This comparison ensures metrological traceability back to the primary measurement standards maintained by a national metrology institute (NMI) [6].

The Airborne Prism Experiment (APEX) was an airborne dispersive push broom imaging spectrometer developed by a Swiss-Belgian consortium for the European Space Agency (ESA) [7]. It was intended to serve as a simulator and a calibration and validation device for spaceborne hyperspectral imagers. Additionally, the APEX provided high-quality remote sensing data for the European EO community, outputting hyperspectral data cubes with 1000 across-track pixels, 532 spectral bands in full spectral mode, and 312 spectral bands after binning some bands in the visible and near-infrared (VNIR) covering a wavelength range from 372 to 2540 nm [8] (i.e., most of the solar reflected spectrum). The APEX calibration measurements were carried out at the German Aerospace Center (Deutsches Zentrum für Luft-und Raumfahrt, DLR) Calibration Home Base (CHB [9]) laboratory in Oberpfaffenhofen, Germany. Given the instrument's role, its proper calibration and characterization were paramount, and the laboratory calibration of the APEX has been the subject of previous publications [8,10,11]. In this paper, we focus on spectroradiometric calibration. Spectral calibration defines the spectral sensitivity of each pixel of the instrument. The main output of radiometric calibration is the absolute spectral responsivity (sometimes referred to as the "radiometric gain") for each pixel. The radiometric coefficients not only are affected by the spectral sensitivity, but also can depend on pressure and temperature conditions, the dark current, and smearing effects; any binning of spectral bands must be compensated before the coefficients can be extracted in a repeatable way. The APEX was retired from operational use in late 2019; however, we had started some preliminary work for a potential simultaneous spectroradiometric calibration, which would require a new calibration facility. In addition, the processing pipeline needed to be adapted and tested for what

would effectively amount to a paradigm shift in the approach to the instrument's spectroradiometric calibration.

The National Physical Laboratory (NPL [12]), the United Kingdom's national metrology institute, recently developed the transportable Spectroscopically Tunable Absolute Radiometric, calibration and characterisation, Optical Ground Support Equipment (STAR-cc-OGSE) [13] to provide a means for the pre-flight calibration and characterization of satellite sensors operating in the ultraviolet, VNIR, and short-wave infrared (SWIR) wavelength range (270–2500 nm). Moreover, the NPL is currently developing sister facilities for the calibration of small satellites, airborne, and ground instruments such as field spectroradiometers. STAR-cc-OGSE is fully traceable to the SI [3,4] via the NPL's primary radiometric standard, the cryogenic radiometer. The facility's laser systems can be used to perform a single high-resolution scan of all the imager's spectral bands, which can allow for the simultaneous retrieval of both spectral and radiometric coefficients for all across-track pixels. Though initially envisaged, an actual spectroradiometric calibration of the APEX with the STAR-cc-OGSE facility was not feasible, with the STAR-cc-OGSE only being recently repatriated from Airbus Toulouse to NPL London [14]. Hence, we opted to simulate the process using the APEX sensor characteristics as a case study. The following sections first describe the methodology used for the actual laboratory spectroradiometric calibration of the APEX imaging spectrometer, then elaborate on the principles and implementation of a simulated simultaneous spectroradiometric calibration of the APEX using the STAR-cc-OGSE facility.

2. METHODS

A. Spectroradiometric Calibration Overview

Laboratory spectroradiometric calibration of either imaging or non-imaging spectrometers has typically relied on performing two separate sets of measurements: one for spectral calibration, and another for radiometric calibration [15,16]. In order to reasonably ensure that the instruments do not undergo changes in their internal state, these two sets of measurements need to be carried out in close succession (avoiding rough transportation in the intervening time) and under the same environmental conditions.

The main aim of spectral calibration is to define the wavelength-dependent instrumental spectral response function (ISRF) of the instrument on a per-pixel basis. The ISRF can be understood as the convolution of the slit image, the detector spatial response in the spectral direction, and the optical point spread function [17]. The ISRF is defined by a center wavelength (CW) position (i.e., the wavelength halfway between the two points with a spectral density of 50% of the peak; the CW corresponds to the peak response wavelength for a symmetrical spectrum) and a response shape [18], and hence is a relative spectral responsivity (the amplitude is arbitrary). ISRFs are most commonly parameterized using the standard Gaussian [17–20], with the associated full width at half maximum (FWHM) being used to express the spectral resolution. The spectral data required for ISRF parameterization can be obtained by using emission line lamps or a scanning monochromator/laser. The need for ISRF parameterization stems from a common limitation: the unavailability of a tunable laser capable of covering the full wavelength range of a VNIR-SWIR spectrometer. Hence, the measured spectral shapes at specific bands have to be interpolated across all the remaining bands in order to obtain the complete wavelength-dependent response of the instrument.

Radiometric calibration ultimately aims to convert the digital number (DN) output into physical units. Specifically, the radiance response of each spectral band is ascertained by determining the conversion coefficients between the DNs and the (nominally) uniform-radiance field at the instrument's entrance pupil, which is commonly assumed to be a linear sensor system [19]. Typically, the radiometric measurements are carried out using the output of an integrating sphere acting as a reference radiation source [21]. The integrating sphere radiance measurements are performed at various intensities, and the result of the calibration is the *absolute spectral responsivity* and the associated offset per band and per spatial pixel based on a linear fitting of the DNs (normalized for integration time) for the various sphere intensities.

With the recent development of the STAR-cc-OGSE facility, a simultaneous spectroradiometric calibration becomes possible using a tunable continuous-wave laser with an SI-traceable output. In this case, a single scan of the entire VNIR and SWIR wavelength ranges with a high spectral sampling frequency is sufficient for the accurate determination of the ISRF coefficients and absolute spectral responsivities (see Section 2.C.3).

B. Laboratory Spectroradiometric Calibration of APEX

1. Spectral Calibration

The original research plan foresaw a spectral calibration of the APEX instrument using a tunable laser fed into an integrating sphere overfilling the FOV of the APEX in order to characterize all spatio-spectral pixels of the instrument (536 × 1000) [22]. However, the DLR had not yet finalized the setup at the time the data acquisition was foreseen. Due to this, the spectral calibration was based on so-called sampling patterns used to define the ISRF at selected spatio-spectral locations on the sensor chips, with the values in between the measured pixels derived via interpolation.

Measurements: the same spatial sampling positions were chosen for both the VNIR and SWIR detectors, and set at positions 20, 150, 300, 499, 700, 850, and 980 (see Fig. 1). The spectral sampling positions are defined by center wavelengths (CWs), the actual scan width, and the monochromator wavelength steps, which are dependent on the spectral region. The sampling step size was nominally set to 0.2 nm for the lower VNIR (385–600 nm) and to 1 nm for greater wavelengths (600–2498 nm): dividing the VNIR into a lower and upper region was a decision driven by the need for a finer sampling step size where the detector's spectral sampling interval (SSI) is significantly smaller compared to the SSI at greater wavelengths, and the implementation had to account for the specifications of the available gratings for the monochromator. The patterns appearing in the step size plots are a systematic effect of the monochromator, where a requested wavelength is in reality only an approximation. The actual wavelengths that the monochromator could

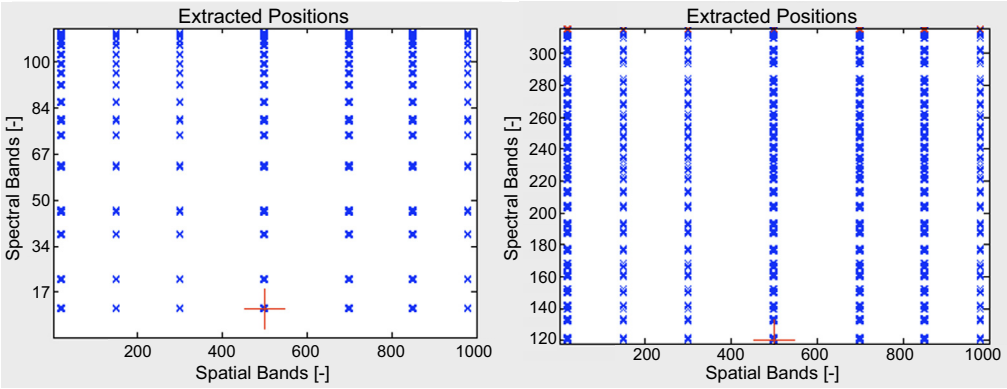

Fig. 1. Extraction positions on the VNIR (left) and SWIR (right) detectors, used for the APEX spectral calibration at DLR's CHB.

set were determined by the CHB's echelle grating wavelength meter [23], and those values were therefore assumed to be the correct ones. The number of spectral sampling positions was set to 16 for the VNIR and 24 for the SWIR. The agreement at the VNIR-SWIR overlap was verified as a sanity check only: this region was not used for calibration as it suffered from the etalon effect [24].

In addition to the spatio-spectral sampling for both detectors, the calibration was complemented by a continuous scan sampling of the ISRF at one defined spatial position, the nadir, through a monotonous increase of the monochromator's wavelength. Given the reliance on calibration routines which did not allow a wavelength-dependent dynamic scan step size, in practice, the VNIR sampling was accomplished using two independent scans to apply different step sizes for the lower (385–600 nm) and higher VNIR regions (600–998 nm). The SWIR detector was sampled between 900–2498 nm with a nominal step size of 0.6 nm.

Extraction of Data for ISRF Characterization: the extraction of ISRF information from the raw frames for the derivation of the CW and FWHM for each spatio-spectral pixel was a computational challenge due to:

- the amount of data prohibiting the loading of the full data set into memory;
- the frames holding the raw ISRF data being essentially a time series where the monochromator wavelength changes over time;
- the raw ISRF data spectral pixel location within the frames being an unknown requiring *a priori* knowledge to extract it;
- the scan intervals actually being large enough to extract the ISRF of neighboring spectral pixels as well;
- the illuminated spot in the across-track direction extending to about 30 pixels, theoretically allowing the extraction for several across-track pixels centered around the target pixel, but since this is constrained by the monochromator spot displaying a wavelength bending due to the projection of the exit slit, using these surrounding pixels was deemed impractical;
- the actual ISRFs being only approximated by Gaussian curves, which may lead to wrong estimations of CWs and FWHMs, especially for VNIR wavelengths affected by the etalon effect [24];
- interpolation/extrapolation of CWs and FWHMs to form continuous calibration layers is prone to produce artifacts.

All information extraction taking the above into account was implemented in the spectral calibration module of the APEX calibration information system (APEX CAL IS [11]), which provides an interactive GUI that enables control over the extraction process, including the inspection of each raw ISRF vector, its Gaussian fit, variations across-track (i.e., spectral misregistration or smile), applied fits, and associated residuals, as well as the definition of thresholds for the outlier removal based on the FWHM and R^2.

The extraction of the raw ISRF vector is equivalent to the definition of a 2D vector in an image cube with the coordinates being the spatial position (across-track), spectral position (spectral pixel under consideration), and all acquisitions (frames) with a changing monochromatic wavelength that are relevant for the extraction of the ISRF. While the spatial position is contained in the metadata, the spectral position is a function of the wavelength, i.e., the parameter that is to be determined: to define a spectral pixel position based on the CW of a monochromator scan (the latter determined by the mean wavelength of the scan), an existing calibration cube generated by a different code provided the CW curve which was used as a lookup table by getting the band position closest to the center of the scan. This was based on the search for the highest pixel response on the chip, disregarding faulty pixels.

The relevant frames for the ISRF characterization are given by the frames acquired for a given spatio-spectral sampling position. Data per the target wavelength and spatial position are stored as distinct "spectral groups." For each spectral group, the following extraction process was applied:

1. bulk reading of all dark current corrected frames of the spectral group, building a virtual image cube in memory;
2. loading of the metadata vector holding the monochromator wavelengths;
3. determination of the spatial and spectral extraction position: this is the center pixel of the extraction;
4. definition of the extraction neighborhood: this was set to pixel positions ± 1 pixel around the center pixel;
5. ISRF extraction for all identified extraction positions.

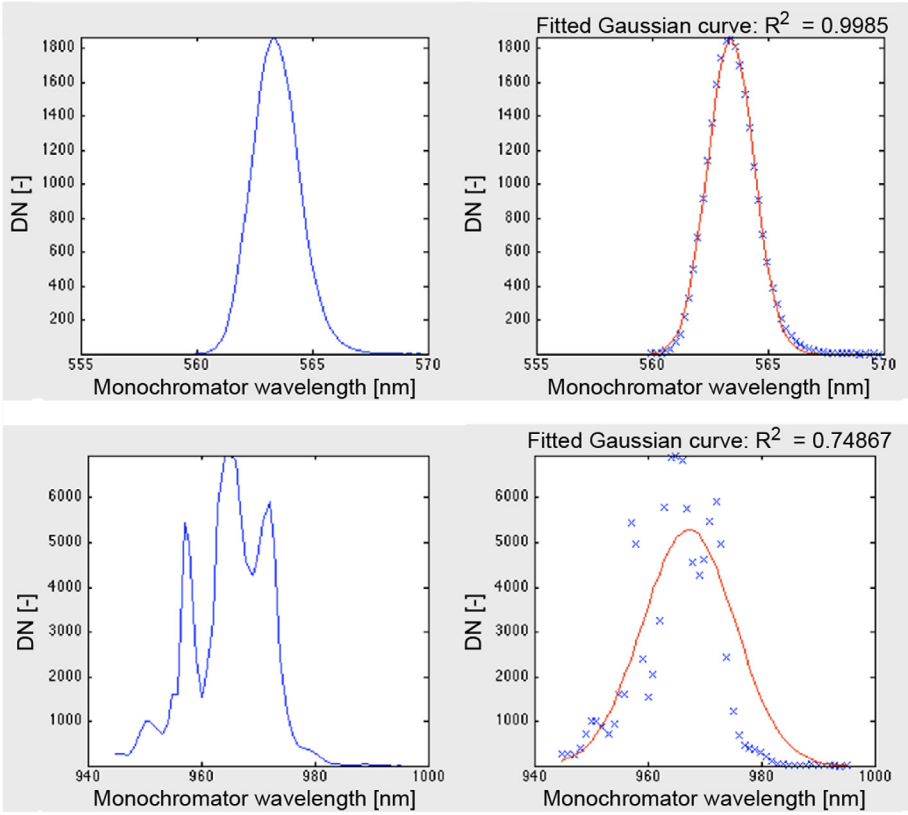

Fig. 2. APEX spectral calibration: optimal Gaussian fit example (top) and suboptimal Gaussian fit example due to the etalon effect (bottom).

For the continuous scan sampling data, the spectral group was defined on the fly: the criterion deciding if enough data points are available is a spectral extraction window defined by the expected CW of a pixel and a buffer size of ±2 FWHM. This criterion was applied to all spectral pixels for the spatial scanning position. Both the CW and the FWHM are estimated based on existing spectral calibration data in the database. Data are loaded into memory based on a sliding spectral extraction window, keeping the data transfer minimal by only loading the delta information required to build the virtual cube per iteration step.

For each identified extraction position within this neighborhood, the following processing is applied:

1. extraction of the raw ISRF vector from the virtual cube;
2. loading of metadata vectors for the following parameters:
   (a) monochromator filter IN
   (b) monochromator filter OUT
   (c) monochromator grating
3. normalization of the raw ISRF vector for changes in monochromator configurations based on the above three parameters. This removes intensity steps in the recorded data due to, e.g., changes of gratings within a scan;
4. fit a Gaussian curve to the normalized ISRF vector and conversion of the standard deviation σ to the FWHM (we applied the three-sigma rule, derived from the Vysochanskij–Petunin inequality for unimodal distributions [25], to ensure that each spectral band supporting the wavelength interval would encompass at least 95% of its ISRF coefficients);
5. applying a filter function to remove implausible or suboptimal Gaussian fits. These may occur when data points are affected by, e.g., etalon effects [26]. The standard filter functions are a FWHM of 15 nm and an R^2 of 0.85 (see Fig. 2).

Spectral Interpolation: spectral interpolation was required to fill any gaps in the spectral direction not covered by the sampling pattern. Averaged CWs and FWHMs per spatial extraction position were interpolated to estimate the CW and FWHM of all spectral pixels.

For both the CW and FWHM, appropriate fitting functions were determined. The functions used for this fitting procedure must approximate the shape of the spectral dispersion and be well behaved within the considered wavelength range. Spline fits are unsuitable for this extrapolation purpose. Finding appropriate fitting functions was based on an Internet service [27] that applies hundreds of functions to the data points and ranks them by R2. The functions were then assessed regarding their monotonic properties and extrapolation behavior. The functions are specific to the detector and the variable (CW or FWHM) to be fitted (see Table 1). For FWHM interpolation to all spectral bands, the corresponding best fitting functions could directly be applied. For CW interpolation, the initial use of the corresponding best fitting functions resulted in large oscillating residuals (due to the Runge phenomenon [28]), requiring a two-step approach whereby the edges of the detector (where usually no

Table 1. Best Fitting Functions per Detector and per ISRF Parameter for Spectral Interpolation to Bands not Covered by the Sampling Pattern

Detector and Variable	Best-Fit Interpolation Function
VNIR-CW	Hyperbolic-like: A*X/(B + X) + C*X + O
VNIR-FWHM	Double Exp. w/Offset: A * exp(B*X) + C * exp(D*X) + E
SWIR-CW	Polynomial 5th order
SWIR-FWHM	Polynomial 5th order

measurements were available) would first be fixed by estimating their values using the aforementioned best-fit functions; then the interpolation of the CW vectors would be carried out using a cubic smoothing spline, significantly reducing the residuals.

2. Radiometric Calibration

The most important output of the laboratory calibration is the radiometric absolute spectral responsivity and offset. Spectral response functions and spectral shift characteristics of the instrument are vital in establishing the radiometric coefficients.

The radiometric calibration of the APEX must be carried out under standardized conditions, requiring corrections for pressure and temperature related effects that change the radiometric and spectral behavior of the system. Furthermore, electronic effects such as the dark current anomaly of the SWIR (known as the "pedestal offset"), and the smearing and binning in the VNIR must be compensated before radiometric coefficients can be extracted in a repeatable way. Consequently, the traceability chain for the laboratory calibration has been extended (see Fig. 9).

Measurements: the APEX radiometric calibration concept had undergone a change in paradigm, as the results of temperature and pressure experiments showed that the instrument was not assuming a default state when being calibrated in the laboratory, but was influenced by the actual pressure and temperature of the system, which differs for each calibration. The same holds true for the spectral calibration.

The realization of this has led to the concept of the nominal, i.e., standardized system state. All measurements taken should be transformed into this standardized space where they can be compared. This concept must be applied to both laboratory and in-flight data, as calibration coefficients will be determined for the defined system state. A standardized spectral calibration was defined by averaging over three years of spectral calibrations.

The transformation of measured frames into the standardized system state is based on models parameterized by sensors measuring temperatures and pressures. Both sensor values and models have associated uncertainties, which define the uncertainty of the DN frame to be radiometrically calibrated.

Radiometric Coefficients: the uncertainties of the gain and offset were computed by a Monte Carlo analysis, varying the uncertainty of both computed at-sensor radiance and the APEX DNs (originating from system noise and shot noise). To ease the integration of these gains, offsets, and related uncertainties in the processing and archiving facility (PAF [10]) side of operations (where the conversion coefficients for both system and data calibration had to be retained in memory), the fitting was carried out with DNs on the x axis (Fig. 3). In a purely modeling context, the DNs should be the dependent variable.

C. Simulation of a Simultaneous Spectroradiometric Calibration

1. Overview

The first step is to ensure that our spectroradiometric calibration algorithms function correctly: for this purpose, we conducted a "unit test" simulation using a modeled APEX sensor with known ISRFs and absolute spectral responsivities, and verified that the code could accurately retrieve these measurands from the sensor synthesized DNs.

Before the actual spectroradiometric calibration of the APEX instrument, we simulate the acquisition of measurements by modeling the sensor response to (1) a monochromatic wavelength scan and (2) a broadband spectrum at different intensities (emulating the approach used historically). Thus, forward modeling is carried out, using an instrument model for the VNIR and SWIR sensors on the one hand, and using an imported spectrum covering the same wavelength range on the other hand. In practice, the APEX model's parameters are based on real data: e.g., the CWs, FWHMs, and radiometric coefficients for every spectral band of every spatial pixel as determined through the historical laboratory calibration approach, as described in Section 2.B. Likewise, the NPL provided the SI-traceable STAR-cc-OGSE broadband radiance spectrum for use in this simulation [see Fig. 6(a)].

Next, we showcase how a simultaneous spectroradiometric calibration could be done using the slit scattering function (SSF) method: by performing a single monochromatic wavelength scan of a spectral band at a high spectral sampling frequency, we can retrieve both the band's ISRF coefficients and its absolute spectral responsivity $R(\lambda_{CW})$. This bypasses the need to take broadband spectrum measurements at various intensities and, while a traditional radiometric calibration could be done with only a single bright level measurement and dark measurement if the linearity of the sensor response is separately established, with the SSF method there is no need for the assumption of a linear sensor response. We then tune the spectral sampling frequency and repeat the scanning process multiple times to determine the optimal monochromator/laser wavelength step size for accurately retrieving $R(\lambda_{CW})$, by comparing the latter's values to that of the modeled sensor's predefined responsivity. Utilizing the STAR-cc-OGSE facility for this purpose would allow for the measurands to be traceable to the SI.

2. APEX Spectroradiometric Calibration Simulation: Unit Test

Forward Simulation: programmatically, the forward simulation relies on four distinct Python scripts (see also Fig. 4):

- *run_experiment*: this is what the user initiates to get the simulation running; the script loads the external broadband spectrum, and calls various functions from the *utils_calibrate* and *apex* scripts to define the APEX model instance and simulate the instrument's response under input spectra;

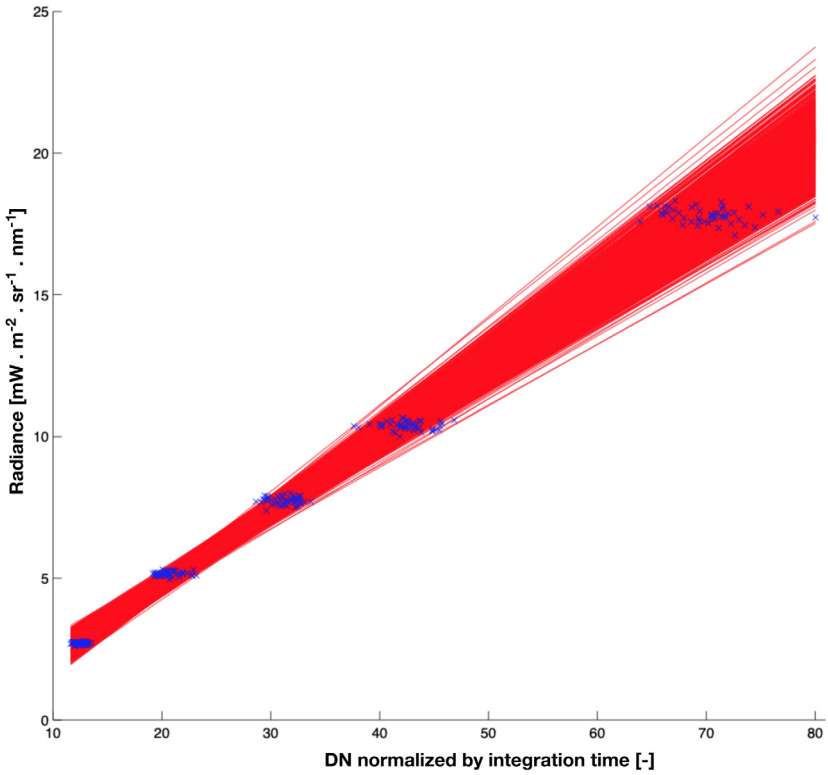

Fig. 3. Straight line fitting Monte Carlo realizations for APEX band 8.

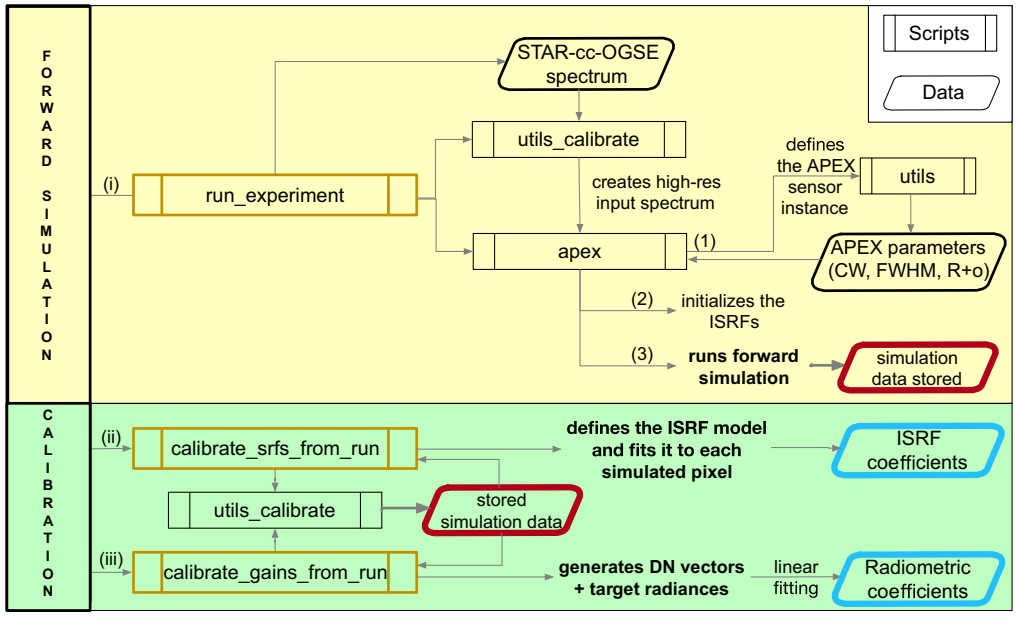

Fig. 4. Processing flowchart for the APEX spectroradiometric calibration simulation.

- *utils_calibrate*: provides a variety of functions, e.g., for creating a high-resolution spectrum from the inputted one, then generating DNs for each spectral band in each pixel;
- *apex*: creates APEX models and stores them (mostly for caching purposes);
- *utils*: defines generic functions for parameter loading and preprocessing, including support for parallel processing of tasks using the Python [29] Joblib [30] library.

The historical APEX parameters are stored in MATLAB [31] *.mat* files as structured arrays, which are converted to dictionaries upon loading the data via *utils*. For a given APEX hyperspectral data cube, the CWs, FWHMs, and radiometric coefficients are loaded. At the same time, a new set of wavelengths with more samples per nanometer is generated such that the input broadband spectrum can be resampled to a higher

resolution using cubic spline interpolation. This step is necessary for the simulation, as the NPL-supplied spectrum only has a radiance value every 10 nm; we settled on three samples per nanometer, which is sufficient for this simulation given that, even in the VNIR, the APEX's SSI is never better than 2 nm and is generally more than double that value, with corresponding FWHMs of over 3 nm at best. Thereafter, different intensity factors scale the resampled input spectrum to simulate a series of measurements for various integrating sphere outputs in order to simulate a traditional radiometric calibration with the linear fitting of the DNs across their corresponding radiances.

In preparation for a spectral calibration free of any ISRF interpolation, an ensemble of monochromatic input spectra with uniform intensities (normalized) is constructed from the pseudo-Dirac delta peaks of the resampled input spectrum, allowing us to simulate a monochromatic scan of all the spectral bands. This would be the scenario where a tunable continuous-wave laser is available for the calibration measurements (see Section 2.C.3). For the ISRF computation (effectively the convolution of the input spectrum with the simulated sensor [32], which can otherwise be described as a weighted average [33]), the ISRFs for each pixel are computed at the resolution of the sensor model's pixel-dependent SSI, within the limits of each spectral band's supporting wavelength interval expressed in terms of standard deviations (we used the three-sigma rule [25].) ISRFs can be binned to account for the binning of VNIR bands.

The APEX model instance is further configured beyond the loading of historical calibration coefficients: the number of across-track pixels (1000), the number of SWIR bands (199), and the number of unbinned (337) and binned (117) VNIR bands are all set in the *apex* script. In practice, the binned VNIR mode is used (the imported parameters also correspond to the binned case), and the VNIR and SWIR bands are gathered into one simulated sensor. Depending on the imported spectrum's range, only a "chunk" of all the APEX model spectral bands is considered (by determining where the "illuminated" spectral bands are).

The *apex* script also contains the function which converts the convolved radiance values to DNs, using either the predefined radiometric coefficients from the sensor model or custom ones provided as arguments (for the purpose of this demonstration, we always rely on the historical calibration data.) The function handles both binned and unbinned data. This is done on a per frame, per intensity factor basis.

Moreover, dark current and signal-to-noise ratio (SNR) models are defined, which also rely on historical APEX data. The dark current coefficients are equivalent to the "absolute spectral responsivities" and associated offsets for each spectral band in each pixel in the absence of incident radiations [34]. The SNR coefficients for each spectral band were derived from calibration measurements carried out under different illumination conditions, and highlight in particular the uncertainty affecting the start and end of the SWIR bands due to the combination of a low SNR, the uncertainty of the dichroic coating, and the effect on temperature, as well as radiometric uncertainty that traces all the way back up the APEX calibration chain to the primary standard maintained at the German Physikalisch–Technische Bundesanstalt (PTB) [35].

The APEX image noise is subsequently generated for each spectral band by first dividing the simulated DNs by the SNR coefficients' absolute values (the noise standard deviation), and then multiplying the result by a random array of normally distributed values with the same shape as the SNR array, such that each run generates a different noise realization (effectively an in-built Monte Carlo method).

Finally, a smear function applies a smearing effect to the simulated VNIR bands, as their physical counterparts rely on a CCD camera (the smearing would arise due to the movement of the sensor or the scene being imaged during a shutterless operation of frame-transfer CCD detectors [36]): the function handles both binned and unbinned data, unbins the data if necessary, calculates the smearing effect, and then rebins the data if it was originally binned. The differential radiance per band is calculated using the integration time and the output from the convolution of the inputted spectrum with the sensor model instance: the cumulative sum of the differential radiance is then used to scale the simulated results. As with other simulated parameters, the smear function is informed by previous APEX calibration and characterization work, including the uncertainty analysis of the instrument's DNs, with the smear correction uncertainty estimated to be at about 1%. No such correction is performed for the SWIR bands: this is not to say that CMOS detectors do not suffer from an effect equivalent to smearing (known as banding or streaking), but it will only become visible in cases where a very bright source is superimposed against a very dark background, an unlikely event in the context of the APEX's daytime Earth observation missions, with any banding effectively falling below the noise floor (unless imaging water and a vegetated shore simultaneously, with near-zero water reflectance in the SWIR).

The forward simulation results, namely, the output from the broadband convolution with the sensor (i.e., the APEX image frames), the corresponding spectral band indices, the simulation configuration, and the ensemble of convolved monochromatic input spectra, are organized into dictionaries and then stored for use in the calibration process.

Spectroradiometric Calibration: for spectral calibration, we run the *calibrate_srfs_from_run* script, which first calls *utils_calibrate* in order to load the forward simulation results, then defines the ISRF model as a Gaussian function (with an offset) and proceeds to fit it to the (pseudo) Dirac delta peaks (one wavelength per frame) for each simulated pixel. The fitting process is performed in chunks to circumvent limitations on the number of parameters that can be simultaneously fitted by the *scipy.optimize.curve_fit* function. In principle, since the inputted monochromatic spectra are interpolated from the NPL-certified STAR broadband spectrum, the calibration wavelength values are directly traceable to the SI, and the outputted CWs and FWHMs from the ISRF fitting process for all bands are sufficient for fully characterizing the APEX sensor model's spectral performance.

At the end of the forward simulation, the convolved APEX frame values have already been converted to DNs from radiance. For radiometric calibration, the *calibrate_gains_from_run* script rearranges the data: programmatically, for each spectral band, the frames are stacked in order to retrieve all the DN values across all spatial pixels, with a function returning a list of DN

vectors for each band. Another function sorts out the target radiance values for each band based on the input spectrum (and the intensity factors scaling the latter). A target radiance value of a specific band is the interpolated radiance value at the mean wavelength of said band. Finally, the process fits a linear model to the DN and target radiance data on a per spectral band basis for all pixels: the slope of a fitted line represents the absolute spectral responsivity for a band with the center wavelength *CW* in pixel i, $R_i(\lambda_{CW})$ (sometimes also referred to as the "gain," for expediency). The result of the linear fits [$R_i(\lambda_{CW})$ and associated offsets] constitute the radiometric coefficients.

3. Simultaneous Spectroradiometric Calibration and the Slit Scattering Function Method

The STAR-cc-OGSE [13] NPL-developed facility provides not only an integrating sphere's broadband source, but also fully tunable continuous-wave laser systems from M Squared lasers that allow for monochromatic scans covering the full VNIR and SWIR wavelength ranges. The scanning laser produces a quasi-perfect monochromatic output, with a wavelength line width of less than a picometer and a laser wavelength position known to within a picometer (traceable to the SI). As a cross-check, the monochromatic wavelength is monitored with another calibrated spectrometer or wavelength meter. Moreover, the STAR-cc-OGSE features thermal-vacuum (TVAC) photodiodes (Si and InGaAs photodiodes to cover both VNIR and SWIR) which take readings alongside the instrument under calibration: the TVAC photodiodes are calibrated to the NPL's primary radiometric standard, which makes it possible to rely on the them as a "transfer radiometer" to determine the radiance measured by the sensors being characterized. With this system, it is theoretically possible to scan the entire wavelength range covered by the APEX instrument with a sufficiently fine laser wavelength step size to spectrally overfill (i.e., fully illuminate) the bands and effectively perform an SI-traceable simultaneous spectroradiometric calibration by retrieving the ISRF and radiometric coefficients without having to repeat measurements at different intensity levels.

We refer to this approach as the slit scattering function (SSF) method for historical reasons because, while it directly profiles the instrument's ISRF, using tunable lasers for scanning a spectrometer was previously proposed as a way of correcting spectral stray light errors [37], and in that context, the relative spectral responsivity (i.e., the ISRF) was referred to as the SSF when each pixel of the sensor is treated as a fixed narrowband filter radiometer, while the wavelength of the incident monochromatic source changes [38].

The following details how the SSF approach to spectroradiometric calibration can work using the STAR-cc-OGSE. After data acquisition (see Fig. 5 for an overall workflow diagram), the imaging spectrometer's system calibration begins with the conversion of the TVAC voltage measurements to radiance:

$$\bar{U}_{\mathrm{TVAC}(\lambda_{\mathrm{laser}})} = \frac{\sum_1^n U_{i,\mathrm{TVAC}(\lambda_{\mathrm{laser}})}}{n}, \tag{1}$$

$$L_{\mathrm{TVAC}(\lambda_{\mathrm{laser}})} = \frac{\bar{U}_{\mathrm{TVAC}(\lambda_{\mathrm{laser}})}}{\gamma_{\mathrm{amp}}} * \rho_{\mathrm{TVAC}}(\lambda_{\mathrm{laser}}) * \alpha_{\mathrm{TVAC}}, \tag{2}$$

where γ_{amp} is the gain of the TVAC amplifier, and $\rho_{\mathrm{TVAC}}(\lambda_{\mathrm{laser}})$ and α_{TVAC} are the photodiodes relative and absolute calibration coefficients.

Similar to Eq. (1), we calculate the mean APEX DN spectra $\bar{y}_{\mathrm{DN}}$ per pixel and per laser tuning step. Obtaining 30 readings per step is a reasonable compromise between the competing interests of acquiring more readings to improve the SNR on the one hand and optimizing the process by limiting the amount of time spent at each laser wavelength step. The result is then normalized for integration time τ and laser power:

$$\bar{y}_{\mathrm{DN\_normalized}(\lambda_{\mathrm{laser}})} = \frac{\bar{y}_{\mathrm{DN}(\lambda_{\mathrm{laser}})}}{\tau * L_{\mathrm{TVAC}(\lambda_{\mathrm{laser}})}}. \tag{3}$$

We obtain the ISRF by fitting a Gaussian to $\bar{y}_{\mathrm{DN\_normalized}(\lambda_{\mathrm{laser}})}$, per band and per pixel. We use the following Gaussian form:

$$G(\lambda_{\mathrm{laser}}) = H + A * \exp\left[\frac{-(\lambda_{\mathrm{laser}} - \lambda_{\mathrm{CW}})^2}{\left(\frac{2*\lambda_{\mathrm{BW,FWHM}}}{2\sqrt{2\ln(2)}}\right)^2}\right] \tag{4}$$

with the following parameters: offset/height H, amplitude A, center wavelength λ_{CW}, and the bandwidth FWHM, since the standard deviation of the Gaussian is $\sigma = \frac{\lambda_{\mathrm{BW,FWHM}}}{2\sqrt{2\ln(2)}}$.

A suitable wavelength interval for the fitting process needs to be established for each spectral band: this is achieved by isolating the maximum (normalized) DN count across all bands per pixel for all laser tuning steps and defining a wavelength buffer on either side of the peak. The buffer can be defined as $\lambda_{\mathrm{laser}}(y_{\mathrm{pixel\_maxDN}}) \pm 3\sigma$, where the standard deviation is spectral band dependent (since the bands have different FWHMs). We then fit the Gaussian to each band's peak and retrieve the CW and FWHM per band and per pixel.

Our best estimate of the absolute spectral responsivity for a spectral band with a center wavelength λ_{CW} in pixel i, $R_i(\lambda_{\mathrm{CW}})$, is obtained by integrating numerically the normalized DNs about the CW (determined by the Gaussian fit):

$$R_i(\lambda_{\mathrm{CW}}) = \sum_{i=\lambda_{\mathrm{CW}}-3\sigma}^{\lambda_{\mathrm{CW}}+3\sigma} \bar{y}_{\mathrm{DN\_normalized}(\lambda_{\mathrm{laser}})}, \tag{5}$$

which requires a fine laser wavelength step size to be accurate.

SSF Method Demonstration: Polygain vs Monogain Study: to demonstrate the validity of the approach, we performed a simulation of the SSF method for a single pixel, single-band sensor with the following characteristics (arbitrary, but representative of the range of characteristics encountered for the APEX case study):

- a Gaussian ISRF of the following form: $g(x) = \frac{1}{\sigma\sqrt{2\pi}} \exp[\frac{-(x-\lambda_{\mathrm{CW}})^2}{2\sigma^2}]$, extending $\pm 3\sigma$ about λ_{CW};
- $\lambda_{\mathrm{CW}} = 500$ nm, and the FWHM = 6 nm;
- an absolute spectral responsivity referred to as the *polygain* parameter (P), i.e, the broadband spectrally flat response that would be obtained from a radiometric calibration using polychromatic (white light) source measurements at different intensities; this parameter is assigned a value of 10.

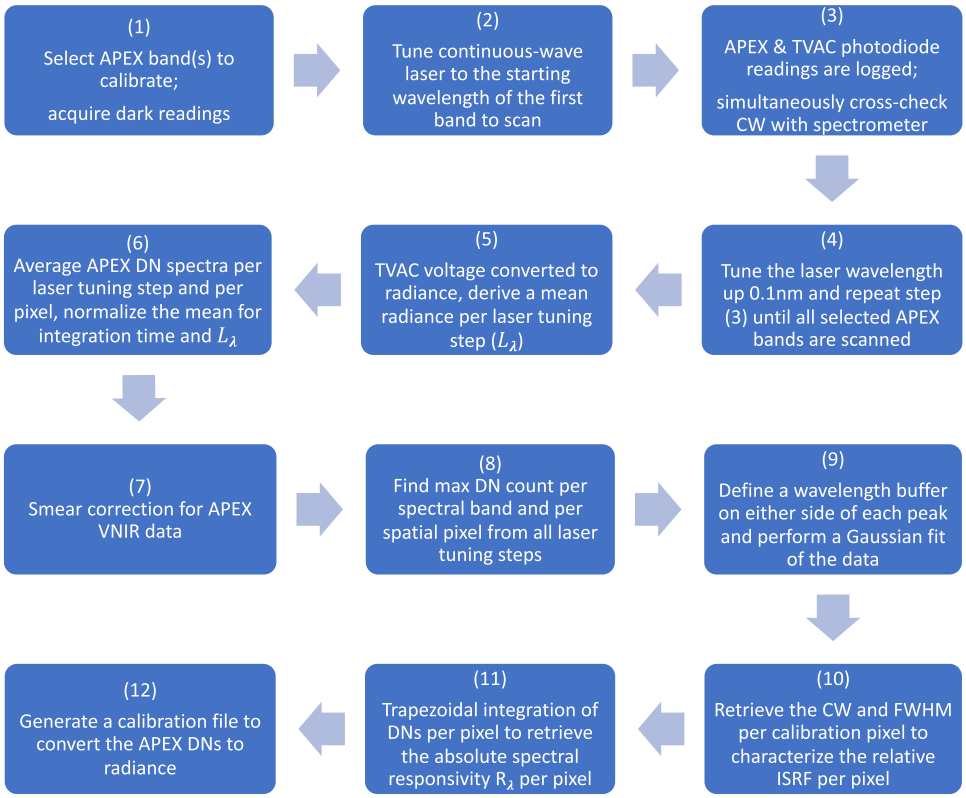

Fig. 5. Workflow for a STAR-cc-OGSE-based simultaneous spectroradiometric calibration of the APEX imaging spectrometer using the SSF method.

In order to define the simulation's at-sensor radiance, the input laser source is assigned an arbitrary constant radiance value of $L_{\text{laser}} = 3.3 \cdot \text{W} \cdot \text{nm}^{-1} \cdot \text{sr}^{-1} \cdot \text{m}^{-2}$, and the DNs that would result from white light measurements would be equivalent to $y_{\text{poly\_DN}} = L_{\text{laser}}/\text{P}$ (assuming the *polygain* signifies the total efficiency of the electro-optical system).

The laser scanning is simulated by defining a scan vector across a wavelength interval that encompasses the band's ISRF range, with a wavelength step size δ_λ which we tune for different simulation runs. For a given run, we then loop the generation of the at-sensor radiance converted to poly_DN across the wavelengths of all the scan vectors and convolve the pseudo-Dirac delta peak with the sensor's ISRF coefficients, one step at a time. The resulting synthesized DNs are scaled by the ISRF coefficients as can be seen in Fig. 8(a).

To calculate the absolute spectral responsivity $R(\lambda_{\text{CW}})$, which we will also refer to as the *monogain* (pseudo-Dirac delta response), we perform the integral of the DNs obtained from one monochromatic scan [see Eq. (5)]. In order to determine the ideal wavelength step size for the accurate retrieval of $R(\lambda_{\text{CW}})$, we simulated 1000 scans with sampling step sizes ranging from 5 to 0.001 nm, and compared the resulting values of the *monogains* to that of the *polygain* (the "true" value of the sensor's absolute spectral responsivity, as defined in this simulation). In terms of accuracy, the target requirement is a relative error of 0.01% for $R(\lambda_{\text{CW}})$ (which emulates an initial requirement used for the spectral calibration of the Microcarb spectrometer with STAR-cc-OGSE, in view of a final calibration uncertainty of below 0.5% [39]). We then repeated the simulation for different FWHMs to cover the range of APEX VNIR and SWIR values, and establish the optimal spectral sampling step size for each case using the same accuracy requirement.

3. RESULTS

From the simulation of the APEX spectral calibration, we retrieved the CWs and FWHMs from the ISRF fitting process for all spectral bands in every spatial pixel. Figure 6(a) shows the original input radiance spectrum: it was from the resampled version of this input spectrum that an ensemble of normalized monochromatic input spectra was constructed. Figure 6(b) displays the ratios of (normalized Gaussian) ISRF reconstructions (based on the coefficients determined from the simulated monochromatic scans at different intensities) against the ISRF curve derived from the highest intensity factor scan: aside from the extreme case of the ratio with an ISRF derived from a very low brightness scan (three orders of magnitude lower than the baseline intensity factor of 1), this plot reveals residual non-linearities in the spectral band's radiometric response beyond the FWHM region. Crucially, these non-linearities remain significant within three standard deviations of the CW, making the assumption of linearity a source of error for a traditional radiometric calibration.

In order to better visualize the results, Fig. 6(c) reveals the APEX image frame resulting from a fixed monochromatic light input, and Fig. 6(d) shows the corresponding response profile for a selection of three spatial bands. Note that the image

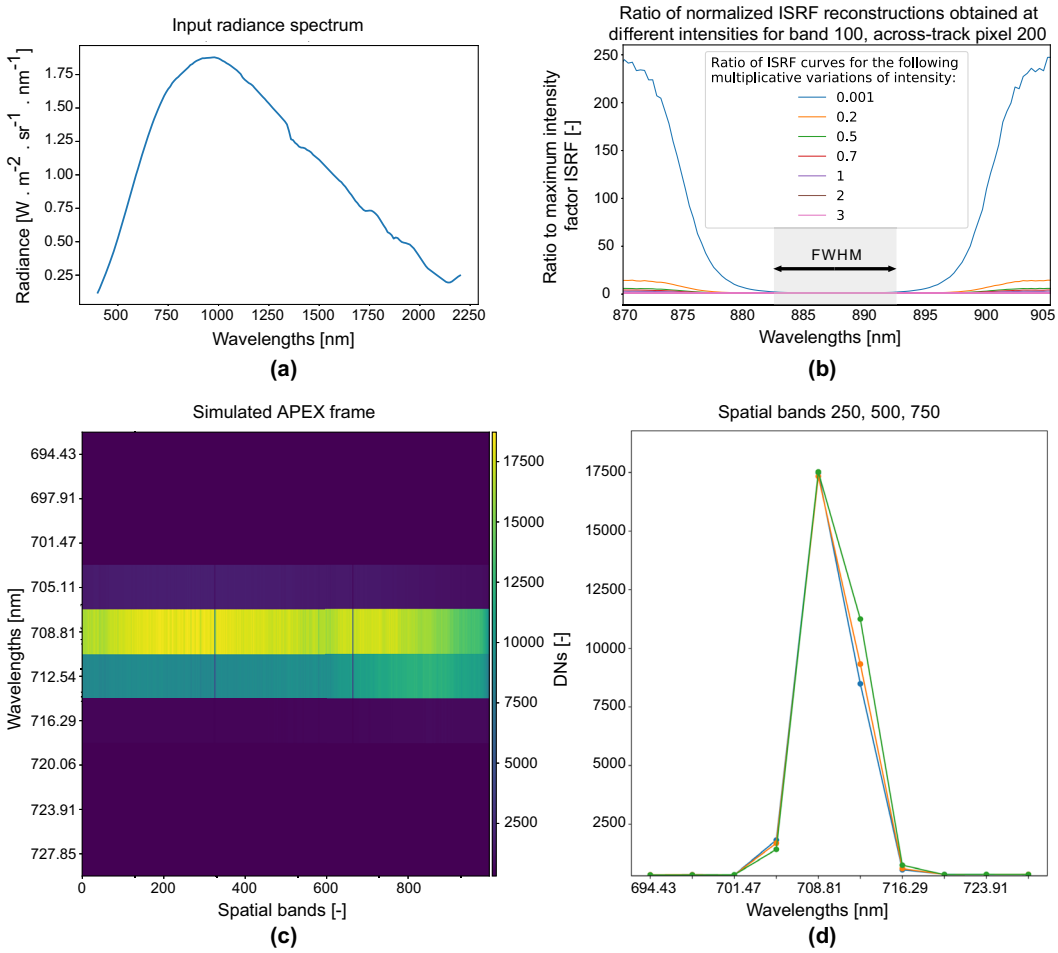

Fig. 6. (a) STAR-cc-OGSE's broadband radiance spectrum used in the simulation of APEX spectroradiometric calibration. The spectrum corresponds to the STAR's large integrating sphere output at 100% intensity. Given this input spectrum covers only the 400–2200 nm wavelength range, the simulation technically only calibrates a "chunk" of the instrument's spectral bands rather than the full 375–2500 nm range. The input spectrum is resampled to a higher resolution for the forward simulation. Normalized monochromatic spectra are derived from the input spectrum for the spectral calibration simulation. (b) Ratio of Gaussian ISRF reconstructions from monochromatic scans of a single spectral band in a single pixel at seven different intensities (intensity factors scaled the resampled input spectrum to simulate measurements at various integrating sphere intensities for the radiometric calibration unit test). Where the ratio is flat, the response is linear: this is mostly the case around the peak response wavelength and beyond for ISRF curves obtained from scans at higher intensity levels; however, residual radiometric non-linearities remain significant within three standard deviations from the band's CW. (c) Simulated APEX image frame from a monochromatic light input and (d) corresponding illuminated bands' DNs for three selected spatial bands.

frame exhibits two distinctly darker lines: these are caused by a residual masking component that was meant to be removed after the instrument's testing was completed, but unfortunately remained for the rest of its operational lifetime. Since the APEX sensor model is instantiated using the calibration coefficients determined historically through laboratory calibration at the CHB, the simulation results retain the quirks.

Based on the broadband spectrum-based calibration simulation, Fig. 7(a) illustrates one result from the fitting of a linear model to the DN and target radiance data on a per spectral band basis for all pixels. Note that while in a pure modeling sense, the DNs should be the predicted variable; the fitting was done with the DNs on the x axis, a holdover from the original APEX calibration approach which also needed to handle uncertainty propagation via a Monte Carlo method (see Section 2.B.2, compare also Fig. 3). Figure 7(b) shows the average absolute spectral responsivity for one spectral band across all pixels, along with the uncertainty due to the APEX noise: even at the 99.7% confidence interval, where the coverage factor is $k = 3$ (for a normal distribution), the envelope is virtually invisible. We observe, again, the effect of the residual masking component in the shape of two highly irregular peaks.

With regard to the simulation of the SSF method, Fig. 8(b) shows the resulting ISRF coefficients as a function of the spectral sampling frequency. With the final aim consisting of determining the optimal laser wavelength step size for accurately retrieving $R(\lambda_{CW})$, Fig. 8(c) illustrates the convergence of the integrated monochromatic responsivity (*monogain*) towards the set value of the spectral band's absolute spectral responsivity (*polygain*) as a function of the laser sampling step size. With a target relative error of 0.01% or better for $R(\lambda_{CW})$, we find that for a band with a FWHM of 6 nm, a 0.2 nm step size is comfortable. [The *monogain* is within 0.005% of the value of the *polygain*; see also Fig. 8(d).] For comparison, other simulations were run with

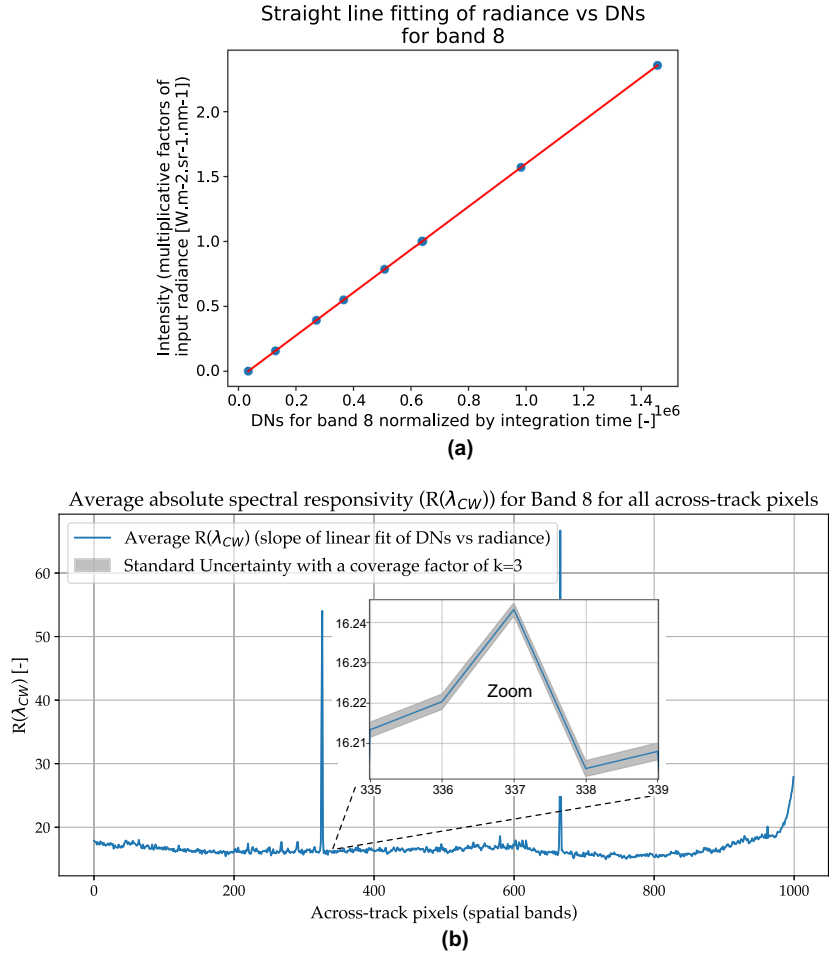

Fig. 7. Results from the simulated radiometric calibration unit test. (a) Straight line fitting for a single spectral band at APEX pixel 500. (b) Average absolute spectral responsivity for the same band across all pixels, along with a zoomed in view to reveal the uncertainty buffer.

the spectral band assigned FWHMs of 3 and 12 nm (about the minimum and maximum for the APEX sensors): in these cases, respectively, 0.1 and 0.4 nm step sizes are sufficient to meet the target requirement.

4. DISCUSSION

A. Historical Approach to the APEX Spectroradiometric Calibration

The method used for the laboratory spectral calibration of the APEX was the result of a compromise: the initial goal had been to fully scan the instrument's spectral bands with a tunable laser, but the unavailability of such a setup at the time led to the so-called sampling pattern approach, where selected spatio-spectral locations were scanned with a monochromatic source, and the ISRF values in between the measured locations were derived via interpolation. It was found that the interpolation algorithm remains the major source of error, as the values measured at the sampling positions fall largely within the uncertainty threshold of the monochromator. The implementation used a constrained smoothing spline-based interpolation, which leads to some artifacts attributable to the Runge phenomenon [28]. This implementation remains superior to the "best-fit" function approach, which results in higher errors when comparing to the continuous scan data. Reducing the effect of these artifacts is not straightforward, however, requiring further investigation of the interpolation method. Another factor which affected the retrieved ISRF coefficients (i.e., both CWs and FWHMs) was the delta pressure of the APEX instrument. This is beyond the scope of this paper, with our simulation not taking into account variations in delta pressure and relying on the STAR-cc-OGSE workflow, which is designed for vacuum, as the system is primarily destined to calibrate satellite instruments. This is in part why the APEX could not be calibrated with the STAR-cc-OGSE; however, the facility was also still under development by the time the instrument was retired from operational use in 2019.

Regarding radiometric calibration using a broadband spectrum measured at different intensities, a major issue stems from the reliance on the assumption of a linear response from the sensor. Like many electro-optical systems, the APEX sensors were designed to have a linear response within a certain range of input radiance (compare also Fig. 3). However, the assumption of linearity remains fundamentally prone to introducing errors in the calibration process, especially towards the edges of the VNIR and SWIR ranges (due to the lower internal quantum efficiency of the detectors' pixels [40]). Correcting for non-linear responses requires more complex models and

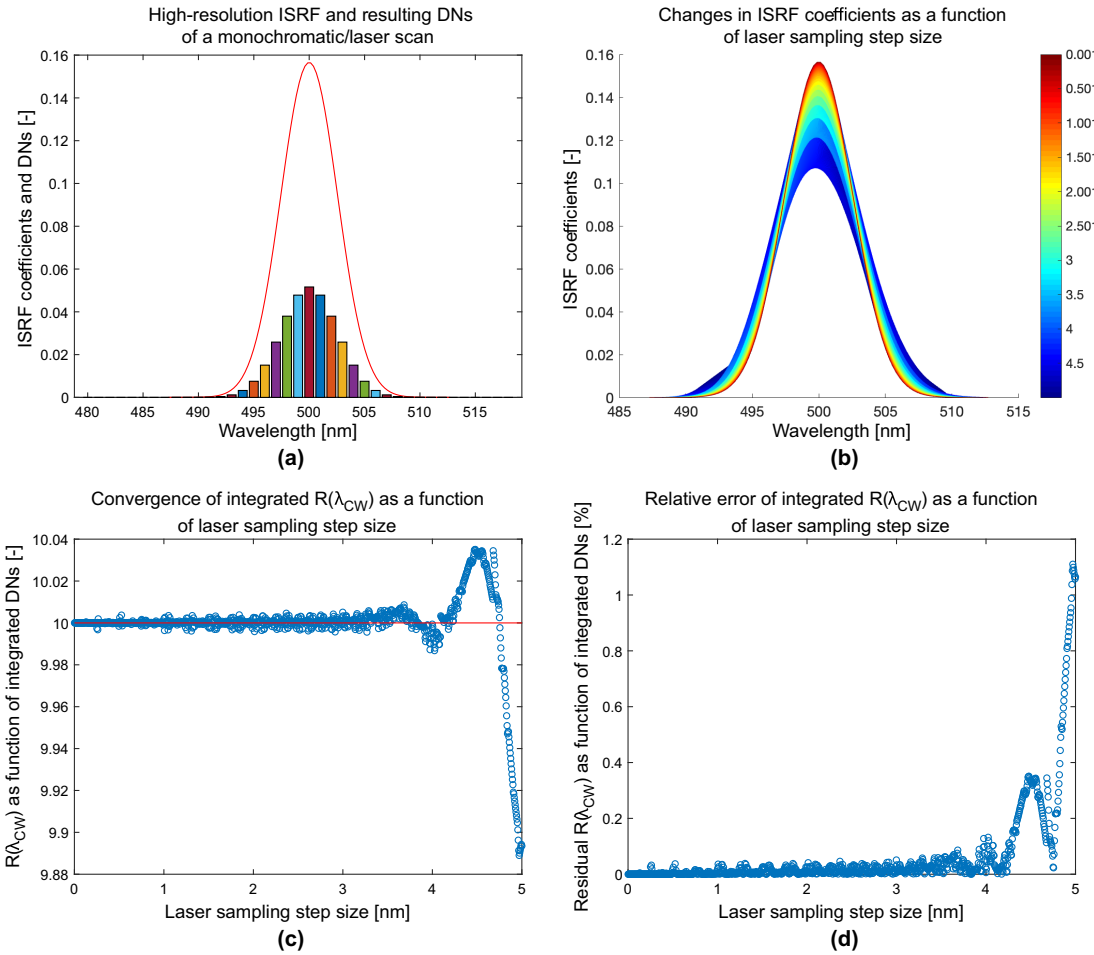

Fig. 8. Results from the SSF method simulation, using a spectral band with a Gaussian ISRF and a FWHM of 6 nm. (a) High-resolution ISRF profile of the simulated single-band sensor juxtaposed with the convolved DNs resulting from a monochromatic scan with a wavelength step size of 1 nm. (b) Color map showcasing how the convolved ISRF coefficients change as a function of the scanning wavelength step size. (c) Convergence of the monochromatic responsivity (*monogain*) - obtained through the integration of the convolved DNs - with the polychromatic responsivity (*polygain*) set to 10 (the "true" value of the absolute spectral responsivity). (d) Relative error of the *monogain* as a function of the laser wavelength step size.

additional calibration steps, increasing the complexity of the data processing pipeline. In turn, non-linear corrections will introduce additional uncertainty into the calibration results, reducing the overall confidence in the data. Although spectral calibration would have benefited from the planned scan of all the APEX wavelengths, radiometric calibration would still have relied on a traditional white light source, as no equivalent to the STAR-cc-OGSE facility existed at the time.

B. Simultaneous Spectroradiometric Calibration and Uncertainty Minimization

The unit test simulation results seem reasonable in that they indicate that our calibration algorithms can, in fact, return the APEX image frames and the ISRF coefficients from monochromatic scans, as well as the radiometric coefficients from the broadband spectrum measurements. Since the main objective of this study was to simulate a workflow allowing us to simultaneously retrieve both ISRF coefficients and absolute radiometric responsivities from a single set of measurements using the SSF method in conjunction with a calibration facility such as STAR-cc-OGSE, the propagation of uncertainty was not prioritized. While the monochromatic scanning covered all spectral bands falling within the wavelength range of the input spectrum, i.e., between 400 and 2200 nm, for all spatial pixels (which is a much greater sampling than what was achieved during the physical calibration of the instrument), we did not set out to compare the differences in ISRF uncertainty between the simulation and the historical results which heavily relied on interpolation. This extra step would make more sense in the context of a new physical spectral calibration with no reliance on previous APEX data. Moreover, a proper uncertainty analysis would require that the uncertainty for the monochromatic source's wavelength is provided, and at the time of this study, the NPL could not supply output data and associated uncertainties from the laser systems (there are several to cover the full 260–2700 nm wavelength range), hence why the normalized monochromatic spectra were generated on the wavelengths of the resampled broadband spectrum. This limitation should be tempered by the knowledge that STAR-cc-OGSE advertises monochromatic sources with a wavelength position known to within a picometer (traceable to the SI) and a line width of under 0.1 pm [13] which, for all intents and purposes, is equivalent to

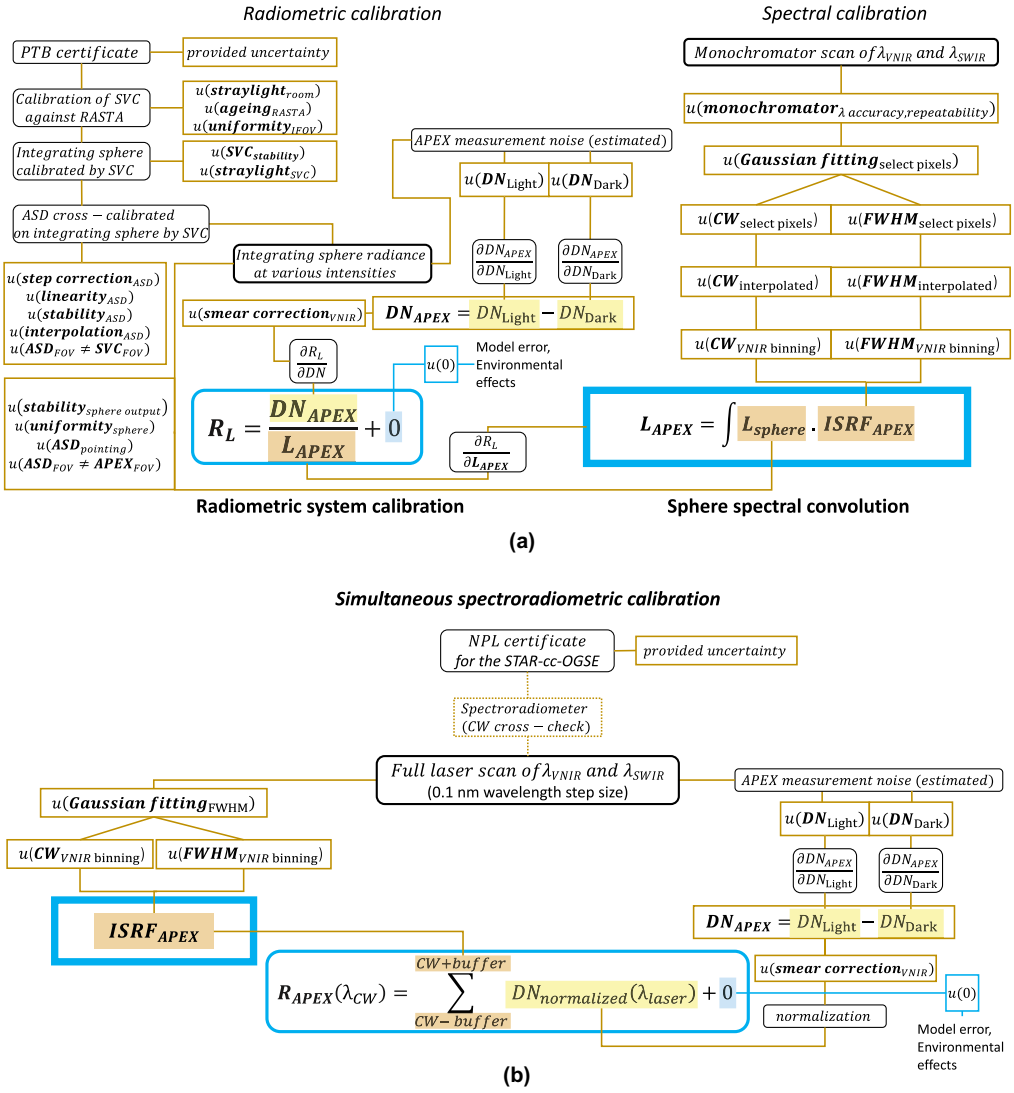

Fig. 9. Uncertainty tree diagrams where the sources of uncertainty and uncertainties are shown in brown boxes. (a) Uncertainty tree diagram for the APEX spectroradiometric calibration based on the historical procedure. The final output is an absolute spectral responsivity and an offset: this is the result of a linear fitting for the various integrating sphere intensities. (b) Uncertainty tree diagram for a simultaneous spectroradiometric calibration of the APEX with the STAR-cc-OGSE using the SSF method. The result is an integrated absolute spectral responsivity which is highly accurate for a fine laser wavelength step size.

a pseudo-Dirac delta function. The added uncertainty would thus be negligible.

The forward simulation does consider the APEX system noise in the DN-domain, which per the central limit theorem (CLT) is assumed to be normally distributed. It remains negligible; however, we only simulated the instrument in the standardized system state (see Section 2.B.2), which does not reflect real measurement conditions. The STAR-cc-OGSE broadband spectrum was provided, along with radiance uncertainty values (with relative uncertainty in the range of 1.5–3.3%), but its propagation would have little value, as we only used the broadband spectrum for the unit test, whereas a quantified comparison of uncertainties between the historical laboratory calibration results and the simulated simultaneous calibration approach would have to consider the uncertainties of the TVAC-derived radiances, which were not available.

Having stated those caveats, there are still a number of qualitative observations that can be made in terms of how a STAR-cc-OGSE-facilitated SSF method minimizes uncertainty compared to performing two separate sets of measurements for spectroradiometric calibration. It is evident that the results from a single series of measurements will incur the effects of fewer sources of uncertainty compared to multiple series of measurements with more than one setup. To illustrate this, we produced uncertainty tree diagrams for both scenarios (see Fig. 9): the first diagram provides an overview of the traceability chain and sources of uncertainty for the APEX laboratory calibration, including the processing for the ISRF fitting, spectral interpolations, preprocessing, and estimation of radiometric coefficients. A simultaneous spectroradiometric calibration results in a much simplified uncertainty tree diagram, as there are fewer sources of uncertainty and fewer interpolations required. Moreover,

fluctuations in the internal state of the instrument between measurements (a particularly critical aspect in the case of the APEX) will tend to increase with more measurements and changes in the setup, and would need to be corrected for. One major advantage of the STAR-cc-OGSE facility is that the TVAC detectors are calibrated to the NPL's primary radiometric standard, minimizing the chain of calibrations where each calibration contributes to the measurement uncertainty, whereas the broadband radiance of a typical integrating sphere will be calibrated using secondary standards. For example, in the case of the APEX, the integrating sphere was calibrated by an SVC [41] spectroradiometer, which in turn was calibrated using the DLR's radiance standard (RASTA) [42]. Furthermore, while the APEX spectral calibration had to rely on ISRF interpolation for the non-calibration bands, the STAR-cc-OGSE laser systems could enable a full scan of the VNIR and SWIR sensors and guarantee the spectrally overfilled condition with extremely fine laser wavelength step sizes (the specifications mention the ability to tune the sampling interval down to a few picometers). The exact spectral sampling frequency can be determined based on an accuracy requirement [see also Fig. 8(d)]. The SSF method is also expected to minimize the uncertainty of the smear correction for the VNIR data, as only monochromatic inputs would need desmearing, i.e., the smear can be well characterized, significantly improving the smear model.

In terms of the radiometric uncertainty, an intrinsic advantage of the SSF method is the non-reliance on the linear sensor response assumption. Since STAR-cc-OGSE can output both broadband light and tunable continuous-wave laser emissions, a future study could investigate the quantitative differences in spectroradiometric uncertainty estimations between the traditional linear fit method (using the broadband spectrum at different intensities) and the SSF method for retrieval of the absolute spectral responsivity per band.

The key feature of the SSF method, namely the ability to precisely "draw" the ISRF coefficients for each spectral band, may be very time consuming, with a full scanning of a 375–2500 nm wavelength range with a 0.1–0.2 nm step size potentially stretching into days depending on integration time settings and SNR requirements, and may be deemed excessive depending on the target accuracy. Thus, it is likely that the interpolation of calibrated ISRF parameters to non-calibration pixels remains relevant, even when the SSF method is otherwise feasible. The availability of STAR-cc-OGSE and its sister facilities under development at the NPL in the near future for commercial use may dictate the feasibility of such studies.

The reliance on the Gaussian assumption for the ISRF is another source of uncertainty which we did not investigate, as the APEX instrument is no longer available for further testing. In principle, however, the ability to sample the ISRF shapes at extremely high resolution can allow for more robust testing of various parameterizations aside from the standard Gaussian. which has been shown to be the largest source of uncertainty in laboratory spectral calibration [32]. Moreover, the SSF method can allow us to go a step further: with the spectrally overfilled condition met, the measured spectral shapes could simply be stored as vectors in a spectral database [43], skipping parameterization altogether and further reducing the uncertainty.

5. CONCLUSION

Using the APEX imaging spectrometer's VNIR and SWIR specifications, we performed the forward simulation of spectroradiometric data acquisition by convolving input spectra with the sensor model's response, and simulated spectroradiometric calibration in two distinct ways: as a simulation of the historical APEX laboratory calibration approach using an SI-traceable broadband radiance spectrum to validate our processing algorithms, and using synthesized monochromatic spectra to run an SSF method allowing for the simultaneous retrieval of both the ISRF coefficients and the absolute spectral responsivities for every spectral band in each spatial pixel. We demonstrated the validity of the SSF method by showing the equivalence between the polychromatic responsivity (*polygain*, derived from the linear fitting of the DNs for various broadband intensities), and the integrated absolute spectral responsivity $R(\lambda_{CW})$ (*monogain*, the integral of the DNs obtained from one monochromatic scan) for a sufficiently high spectral sampling frequency. The results show that for FWHMs of 3, 6, and 12 nm, laser wavelength step sizes of 0.1, 0.2, and 0.4 nm, respectively, will meet the targeted 0.01% relative error requirement. This FWHM-dependent fine tuning will matter in the context of a real SSF-based calibration, as a time-consuming full scan of VNIR and SWIR sensors may have to be balanced against the availability of the calibration facility and other operational constraints.

We also detailed the principles of a simultaneous spectroradiometric calibration traceable to the SI using the NPL's STAR-cc-OGSE. The comparison between the traceability chains of the APEX laboratory calibration and the SSF-based STAR-cc-OGSE calibration concept reveals that the minimization of uncertainty is the main advantage of the latter, even without taking into account the state-of-the-art specifications of its laser systems. A future study could seek to quantify the differences in uncertainty estimations between the *polygain* and the *monogain* by conducting both approaches to radiometric calibration with the STAR-cc-OGSE. Furthermore, the fine sampling of the ISRF shapes is ideal for testing different fitting functions beyond the standard Gaussian, which has been a *de facto* default parameterization of the ISRFs for the APEX and many other spectrometers. Given that interpolating calibrated ISRF parameters to non-calibration bands is expected to remain a viable option when practical constraints limit the amount of SSF scanning, reducing the uncertainty in ISRF fitting would be beneficial.

Finally, we provide access to the source code of the simultaneous spectroradiometric calibration simulation for APEX data via GitHub (see Ref. [44]).

Funding. European Metrology Programme for Innovation and Research (19ENV07 MetEOC-4).

Acknowledgment. The authors thank the National Physical Laboratory (NPL [12]) for providing the STAR-cc-OGSE broadband spectrum used in the simulation.

This work was supported by MetEOC-4. The project 19ENV07 MetEOC-4 has received funding from the EMPIR programme co-financed by the Participating States and from the European Union's Horizon 2020 Research and Innovation Programme.

Disclosures. The authors declare no conflicts of interest.

Data availability. The simulation source code, the APEX instrument parameters, and the STAR-cc-OGSE broadband spectrum are available in Ref. [44].

REFERENCES

1. A. Zahra, R. Qureshi, M. Sajjad, *et al.*, "Current advances in imaging spectroscopy and its state-of-the-art applications," Expert Syst. Appl. **238**, 122172 (2024).
2. B. Zhang, Y. Wu, B. Zhao, *et al.*, "Progress and challenges in intelligent remote sensing satellite systems," IEEE J. Sel. Top. Appl. Earth Obs. Remote Sens. **15**, 1814–1822 (2022).
3. L. Alexander, B. William, B. Luca, *et al.*, "Validation practices for satellite-based Earth observation data across communities," Rev. Geophys. **55**, 779–817 (2017).
4. N. Fox, P. Green, H. Brindley, *et al.*, "Traceable radiometry underpinning terrestrial and heliostudies (truths): a benchmark mission for climate," Proc. SPIE **10563**, 635–643 (2017).
5. C. de Vries, T. Danaher, R. Denham, *et al.*, "An operational radiometric calibration procedure for the Landsat sensors based on pseudo-invariant target sites," Remote Sens. Environ. **107**, 414–429 (2007).
6. Joint Committee for Guides in Metrology (JCGM), "International vocabulary of metrology-Basic and general concepts and associated terms (VIM)," 2012, https://www.bipm.org/utils/common/documents/jcgm/JCGM_200_2012.pdf.
7. K. I. Itten, F. Dell'Endice, A. Hueni, *et al.*, "APEX-the hyperspectral ESA airborne prism experiment," Sensors **8**, 6235–6259 (2008).
8. M. E. Schaepman, M. Jehle, A. Hueni, *et al.*, "Advanced radiometry measurements and earth science applications with the airborne prism experiment (apex)," Remote Sens. Environ. **158**, 207–219 (2015).
9. J. Brachmann, A. Baumgartner, and P. Gege, "The calibration home base for imaging spectrometers," J. Large-Scale Res. Facil. **2**, A82 (2016).
10. A. Hueni, J. Biesemans, K. Meuleman, *et al.*, "Structure, components, and interfaces of the airborne prism experiment (apex) processing and archiving facility," IEEE Trans. Geosci. Remote Sens. **47**, 29–43 (2009).
11. A. Hueni, K. Lenhard, A. Baumgartner, *et al.*, "Airborne prism experiment calibration information system," IEEE Trans. Geosci. Remote Sens. **51**, 5169–5180 (2013).
12. National Physical Laboratory, "Delivering impact," 2024, https://www.npl.co.uk/ (accessed 30 October 2024).
13. P. D. Green, S. Devlin, N. P. Fox, *et al.*, "The STAR-CC-OGSE system for pre-flight sensor calibration," 2021, https://ceoi.ac.uk/wp-content/uploads/2021/April_2021_Challenge_Workshop/STAR-CC-OGSE-system-for-pre-flight-sensor-calibration_SD_20210415-Sean-Devlin-1.pdf (accessed 30 October 2024).
14. J. Schofield, C. Baker, P. Green, *et al.*, "The STAR-cc-OGSE Family - A collection of EO sensor calibration facilities," 2023, https://earth.esa.int/eogateway/documents/d/earth-online/vh-roda-2023_schofieldj (accessed 30 October 2024).
15. H. A. Bender, P. Mouroulis, M. L. Eastwood, *et al.*, "Alignment and characterization of high uniformity imaging spectrometers," Proc. SPIE **8158**, 185–195 (2011).
16. C. Cao, C. Ruiyue, and S. Uprety, "Calibrating a system of satellite instruments," in *Satellite-based Applications on Climate Change*, J. Qu, A. Powell, and M. Sivakumar, eds. (Springer Netherlands, 2013), pp. 151–158.
17. Z. Gao, R. Jia, H. Zhang, *et al.*, "Simulation and analysis of spectral response function and bandwidth of spectrometer," Int. J. Aerosp. Eng. **2016**, 2759121 (2016).
18. P. Mouroulis, R. O. Green, and T. G. Chrien, "Design of pushbroom imaging spectrometers for optimum recovery of spectroscopic and spatial information," Appl. Opt. **39**, 2210–2220 (2000).
19. L. Zhang, C. Huang, T. Wu, *et al.*, "Laboratory calibration of a field imaging spectrometer system," Sensors **11**, 2408–2425 (2011).
20. X. Yu, Y. Sun, A. Fang, *et al.*, "Laboratory spectral calibration and radiometric calibration of hyper-spectral imaging spectrometer," in *2nd International Conference on Systems and Informatics (ICSAI)* (2014), pp. 871–875.
21. A. Prokhorov and L. M. Hanssen, "Numerical modeling of an integrating sphere radiation source," Proc. SPIE **4775**, 106–118 (2002).
22. S. B. D. Schläpfcr, M. Schaepman, and A. Börner, "Calibration and validation concept for the airborne prism experiment (apex)," Can. J. Remote Sens. **26**, 455–465 (2000).
23. A. Baumgartner, "Grating monochromator wavelength calibration using an echelle grating wavelength meter," Opt. Express **27**, 13596–13610 (2019).
24. B.-L. Hu, J. Zhang, K.-Q. Cao, *et al.*, "Research on the etalon effect in dispersive hyperspectral vnir imagers using back-illuminated ccds," IEEE Trans. Geosci. Remote Sens. **56**, 5481–5494 (2018).
25. F. Pukelsheim, "The three sigma rule," Am. Stat. **48**, 88–91 (1994).
26. P. Werle, "Accuracy and precision of laser spectrometers for trace gas sensing in the presence of optical fringes and atmospheric turbulence," Appl. Phys. B **102**, 313–329 (2011).
27. J. R. Phillips, "ZunZunSite3 online curve fitting and surface fitting," https://findcurves.com/.
28. C. Runge, "Über empirische funktionen und die interpolation zwischen äquidistanten ordinaten," Z. Math. Phys. **46**, 224–243 (1901).
29. G. Van Rossum and F. L. Drake, *Python 3 Reference Manual* (CreateSpace, 2009).
30. Joblib Development Team, "Joblib: running python functions as pipeline jobs," (2024).
31. MATLAB, *Version 9.10.0.1613233 (R2021a)* (MathWorks, 2021).
32. S. A. Trim, K. Mason, and A. Hueni, "Spectroradiometer spectral calibration, ISRF shapes, and related uncertainties," Appl. Opt. **60**, 5405–5417 (2021).
33. V. Zanoni, B. Davis, R. Ryan, *et al.*, "Remote sensing requirements development: a simulation-based approach," in *Proceedings of the ISPRS Commission I Mid-Term Symposium 2002: Integrated Remote Sensing at the Global, Regional and Local Scale* (2002), pp. 10–15.
34. N. Ali, S. Attique, A. Rahimi-Iman, *et al.*, "Beyond lead: progress in stable and non-toxic lower-dimensional perovskites for high-performance photodetection," Sustain. Mater. Technol. **38**, e00759 (2023).
35. Physikalisch-Technische Bundesanstalt, "Reference standards," 2024, https://www.ptb.de/cms/en/ptb/fachabteilungen/abt4/fb-42/ag-423/publications-423/reference-standards.html (accessed 30 October 2024).
36. F. A. Iglesias, A. Feller, and K. Nagaraju, "Smear correction of highly variable, frame-transfer CCD images with application to polarimetry," Appl. Opt. **54**, 5970–5975 (2015).
37. H. J. Kostkowski, "Spectral scattering," in *Reliable Spectroradiometry* (Spectroradiometry Consulting, 1997), pp. 57–87.
38. Y. Zong, S. W. Brown, B. C. Johnson, *et al.*, "Simple spectral stray light correction method for array spectroradiometers," Appl. Opt. **45**, 1111–1119 (2006).
39. Metrology for Earth Observation and Climate (MetEOC), "Calibration of the CNES/UKSA MicroCarb optical instrument," 2023, https://www.meteoc.org/wp-content/uploads/sites/35/2023/08/GADS1778-%E2%80%93-MicroCarb-optical-instrument-CS-WEB.pdf (accessed 30 October 2024).
40. A. L. M. Zurita, J. C. Acosta, A. S. Shcherbakov, *et al.*, "Measuring the reflectance and the internal quantum efficiency of silicon and InGaAs/InP photodiodes in near infrared range," Proc. SPIE **6890**, 68900P (2008).
41. Spectra Vista Corporation, "Gather great data in the field," https://spectravista.com/.
42. D. Taubert, J. Hollandt, C. Monte, *et al.*, "Absolute radiometric characterization of the transfer radiometer unit of RASTA in the UV, VIS and NIR spectral range," in *SPIE Remote Sensing* (SPIE, 2013).
43. A. Hueni, K. Mason, and S. Trim, "Uncertainty support in the spectral information system specchio," IEEE J. Sel. Top. Appl. Earth Obs. Remote Sens. **16**, 2668–2680 (2023).
44. S. A. Trim, J. Buffat, and A. Hueni, "Code and data for the simulation of APEX calibration using STAR-cc-OGSE 2024," GitHub, 2024, https://github.com/st2space/METEOCPY_04.11.2024.